Journal of Alloys and Compounds 488 (2009) 79–83

Contents lists available at ScienceDirect

Journal of Alloys and Compounds

journal homepage: www.elsevier.com/locate/jallcom

High thermal stability of soft magnetic (Fe,Co)–Mo–B–C–P–Si metallic glasses

S. Bhattacharya[a,*], E.A. Lass[b], S.J. Poon[a], G.J. Shiflet[b]

[a] Department of Physics, University of Virginia, 382 McCormick Road, Charlottesville, VA 22904-4714, United States
[b] Department of Materials Science and Engineering, University of Virginia, Charlottesville, VA 22904-4745, United States

ARTICLE INFO

Article history:
Received 10 July 2009
Received in revised form 19 August 2009
Accepted 20 August 2009
Available online 31 August 2009

Keywords:
Metallic glasses
Soft magnetic
Thermal stability

ABSTRACT

The effects of metalloids on the thermal stability and magnetic properties of (Fe,Co)–Mo–B–C–P–Si metallic glasses are presented. The alloys exhibit high thermal stability, despite only a 40 K width of the supercooled liquid (SCL) region and a reduced glass transition temperature of 0.55. The amorphous phases and their high saturation magnetization (~1.44 T) and low coercive field (~20 A/m) are retained upon long-term annealing in the SCL region. Temperature–time transformation (TTT) studies and investigation of crystallization properties using transmission electron microscopy confirm the beneficial effect of cobalt on the thermal stability, rendering the present alloys promising for scientific study and soft magnet applications.

1. Introduction

Metallic glasses are a novel class of materials with unique structural and physical properties for scientific study and applications. From the applications point of view, the excellent thermoplastic behavior of metallic glasses in the supercooled liquid (SCL) temperature region offers the possibility of fabricating near-net shaped products [1]. Among the metallic glasses, the Fe-based systems with high glass formability (GFA) are of significant interest for their possible excellent soft magnetic properties and high thermal stability against crystallization [2–5]. Thermal stability is desirable because the glassy phase tends to relax into a structural state with increased local short-range order [6], resulting in the increase in magneto-crystalline anisotropy and deterioration of soft magnetic properties. Particularly, crystallization can occur in the SCL region depending on the relative magnitude of the Gibbs free energy difference and interfacial free energy between solid and liquid phases [7,8]. Therefore, the soft magnetic properties of Fe-based metallic glasses must remain stable upon extended annealing in the SCL region in order to take advantage of the thermoplasticity of these metallic glasses.

The GFA of metallic glasses are considered to be related to the width $\Delta T_x (=T_x - T_g)$ of the SCL region [3], where T_x and T_g are the crystallization and glass transition temperatures, respectively. The larger the ΔT_x, the higher is the GFA. A reduced glass transition temperature of 0.6, where $T_{rg} = T_g/T_l$ and T_l is the liquidus temperature, also indicates good GFA [8]. Although the thermal stability of a glass may be related to the GFA, the relationship between these two properties is unclear. Substitutional effects of metalloids and early transition metals on the width of ΔT_x as well as GFA have been widely studied in different Fe-based metallic glass systems [3,9,10]. However, the thermal stability of these alloys has not been studied systematically. In one study, Shen et al. [3] reported good soft magnetic properties and high GFA with $T_{rg} \sim 0.6$ and moderate $\Delta T_x \sim 34$–47 K in the $Fe_{79-x}Mo_xP_{10}C_4B_4Si_3$ (x = 0–6 at.%) alloy series. The latter alloys could be cast into glassy rods up to 4 mm diameters by copper mold casting. In another study [10], a presumably more stable glassy alloy, $Fe_{75}Mo_2Ga_3P_{10}C_4B_4Si_2$ with a larger $\Delta T_x \sim 60$ K, was found to devitrify into a metastable $(Fe,Mo)_{23}(B,C)_6$ crystalline phase upon annealing at $0.37\Delta T_x$ above T_g for 600 s. The metastable phase decomposed into α-(Fe,Mo) and other iron-metalloid phases when annealed above the crystallization temperature. The effect of cobalt substitution on thermal stability has also remained an area of interest in the Fe,Co-based metallic glasses [11,12]. In the present paper, a systematic study of the thermal stability of (Fe,Co)–Mo–B–C–P–Si metallic glasses with varying metalloid concentrations is performed by annealing the samples at temperatures inside the SCL region. These soft ferromagnetic glassy alloys exhibit high thermal stability, as well as high saturation magnetization ($M_s \sim 1.38$–1.44 T) and low coercive field ($H_c \sim 15$–20 A/m). The resulting M_s and H_c values are retained even after significant annealing times at temperatures deep inside the SCL region.

2. Experimental procedure

Metallic glass ribbons of compositions $Fe_{78}Mo_1C_{10-x}B_xP_{10}Si_1$ (x = 3, 5, 7) and $(Fe_{1-y}Co_y)_{78}Mo_1C_7B_3P_{10}Si_1$ (y = 0.15, 0.2, 0.3) are investigated. The selected alloy constituents are similar to those of some Fe-based bulk glass forming alloys, namely,

* Corresponding author.
E-mail address: sb7uj@virginia.edu (S. Bhattacharya).

0925-8388/$ – see front matter © 2009 Elsevier B.V. All rights reserved.
doi:10.1016/j.jallcom.2009.08.114

$Fe_{79-x}Mo_xP_{10}C_4B_4Si_3$ (x = 0–6 at.%) reported by Shen et al. [3] and $Fe_{76-x}Mo_xC_{10}B_2P_{12}$ (x = 5, 7, 10) amorphous steel alloys reported by Gu et al. [13]. The percentage of boron is varied to optimize the thermal stability. Cobalt is added to one of the alloys to increase saturation magnetization. Alloy ingots of nominal compositions were prepared by arc melting appropriate mixtures of high purity Fe, Co and pre-alloyed Fe_4Mo, Fe_3P, Fe_5C/Fe_4C, FeB, and Fe_9Si. Each ingot was melted 3–4 times on a water cooled copper hearth in high purity argon atmosphere to ensure chemical homogeneity. Parts of the ingots were then remelted and melt-spun to obtain ribbon samples. The ribbons were typically ~0.8–1.0 mm wide and ~15–20 μm thick and several meters long. Thermal analysis was performed using a differential scanning calorimeter (DSC) (DSC 7, PerkinElmer) at a constant heating rate of 20 K/min. Liquidus temperatures of these alloys were analyzed using differential thermal analysis (DTA) (DTA 7, PerkinElmer). Coercive field and saturation magnetization measurements were performed at room temperature using a commercial vibrating sample magnetometer (VSM). For the alloys with Curie temperature (T_c) below T_g, T_c could be detected in the DSC scans. For the annealing study, the as-spun ribbons were cut into 3–4 cm lengths and encapsulated in evacuated quartz tubes. The samples were then heat treated in molten lead at temperatures inside the SCL region, near $T_g + \Delta T_x/2$, for annealing times up to 20 min. Two alloys that exhibited high thermal stability were then selected for further annealing studies at various times and temperatures to obtain partial time–temperature transformation (TTT) plots. Both as-spun and annealed ribbons were analyzed by X-ray diffraction (XRD) using Cu Kα1 radiation (λ = 1.541 Å) (XDS 2000, Scintag Inc.). Transmission electron microscopy (TEM) (2000 FX, JEOL) was utilized to study the microstructure of the two compositions that exhibited high thermal stability after annealing at ($T_g + \Delta T_x/2$) for 20 min. The annealed ribbons were dimpled using a commercial Dimpler (D500i, South Bay Technology) and then ion-milled using a Precision Ion Polishing System (PIPS) (Gatan 691) to make them electron transparent for TEM analysis.

3. Results and discussion

Fig. 1 shows the DSC curves of the amorphous $Fe_{78}Mo_1C_{10-x}B_xP_{10}Si_1$ (x = 3, 5, 7) ribbons. With increasing temperature, a pronounced glass transition is detected in the glassy alloys from a distinct change in slope in the DSC curves with increasing temperature below T_x and a moderate ΔT_x of 40 K is measured. The onset temperature of crystallization increases with an increase in boron concentration from $T_x \sim 728$–743 K in $Fe_{78}Mo_1B_3C_7P_{10}Si_1$ and $Fe_{78}Mo_1B_7C_3P_{10}Si_1$, respectively. The Curie points, characterized by small cusp-like endothermic signals in the DSC plots, also increase slightly from $T_c \sim 585$–593 K on replacing carbon with boron. The observed T_c values are found to be in good agreement with those measured using the VSM. The small variations in T_c are also in agreement with T_c variations observed by Luborsky et al. [14], where T_c is found to decrease slightly on replacing boron by carbon below 79% iron concentration

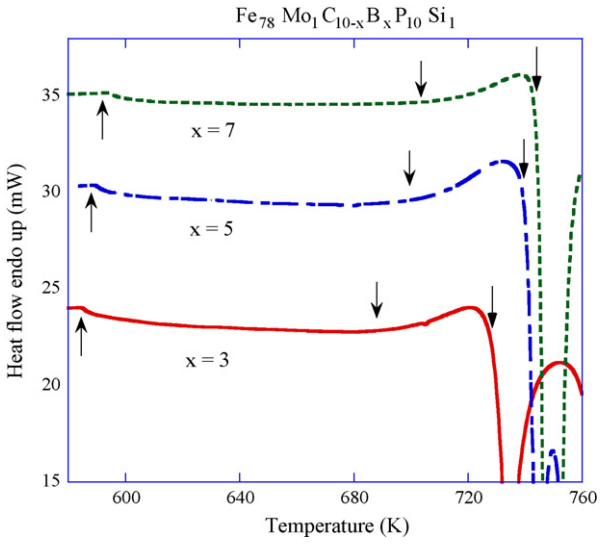

Fig. 1. Differential scanning calorimetric curves of amorphous $Fe_{78}Mo_1C_{10-x}B_xP_{10}Si_1$ (x = 3, 5, 7) ribbons. The (↑) and (↓) arrows indicate T_c and T_g, respectively. The second (↓) indicates T_x.

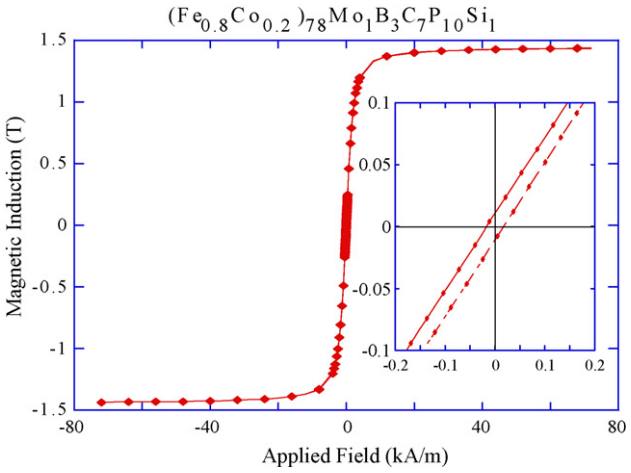

Fig. 2. A characteristic B–H hysteresis loop of $(Fe_{0.8}Co_{0.2})_{78}Mo_1B_3C_7P_{10}Si$, measured at room temperature, with an applied field of 72 kA/m. The inset shows enlarged hysteresis loop near the origin.

in Fe–B–C ternary amorphous alloys. The results are summarized in Table 1. A typical magnetic hysteresis loop of a present composition, $(Fe_{0.8}Co_{0.2})_{78}Mo_1B_3C_7P_{10}Si_1$, measured at room temperature using a vibrating sample magnetometer (VSM) is shown in Fig. 2. The saturation magnetization (M_s) and coercive field (H_c) values extracted from the B–H hysteresis loops are also shown in Table 1. The magnetic field is applied along the longitudinal direction of the ribbon and maximum applied field is usually 72 kA/m, sufficiently large to achieve saturation. The M_s and H_c values obtained are found to be in agreement with those measured in fields up to 1 T. To obtain the hysteresis loop, an applied field, close to H_c, is incremented in step sizes of 16 A/m at low magnetic fields ranging from 0 to ±400 A/m. The field resolution for this range is 0.8 A/m. The H_c measured is low, with a value within the range ~15–20 A/m. The H_c values measured by Shen et al. [3] using a B–H loop tracer were much lower, almost by an order of magnitude. However, a clear discrepancy between H_c values measured by VSM and a B–H loop tracer were reported by Bitoh et al. [15], namely, the H_c of a melt-spun ribbon of composition $[Fe_{0.5}Co_{0.5})_{0.75}B_{0.20}Si_{0.05}]_{96}Nb_4$ measured using a VSM (16 A/m) was significantly higher than that by a B–H loop tracer (3 A/m). The H_c values of the metallic glasses in the present study are thus comparable to those H_c values measured using a vibrating sample magnetometer [15]. M_s increases slightly with increasing boron concentration, retaining a rather high value of 1.42–1.44 T. In order to calculate M_s, the mass density of the amorphous ribbons is estimated using a method based on atomic packing density which will be published in details elsewhere [16]. The calculated mass densities agree within 1–2% of the measured density values of the two present alloys, as well as with other Fe-based metallic glasses. Using this method, the atomic packing density in the (Fe,Co) containing alloys, is found to be slightly higher than the Fe-containing alloys, which will be discussed in more details in [16].

Systematic heat treatments at temperatures near $T_g + 0.5\Delta T_x$, i.e. midway within the SCL region, are performed to determine the effect of boron on the thermal stability of the $Fe_{78}Mo_1C_{10-x}B_xP_{10}Si_1$ (x = 3, 5, 7) series of metallic glasses. Coercive field is measured in the annealed ribbons to determine changes in soft magnetic properties arising due to the onset of crystallization and also due to relaxation of quenched-in stresses in the amorphous structure. On annealing for 15–20 min, the coercivity increases systematically with an increase in boron concentration, as shown in Table 1. With increased boron concentration up to 7 at.%, H_c increases to ~400 A/m after annealing for 15 min. The glassy alloy

Table 1
Summary of Curie temperature (T_c), glass transition temperature (T_g), onset temperature of crystallization (T_x), annealing temperature (T_a), liquidus temperature (T_l), reduced glass transition temperature (T_{rg}), mass density (ρ), saturation magnetization (M_s), and coercive field (H_c).

Composition	T_c (K)	T_g (K)	T_x (K)	T_a (K)	T_l (K)	T_{rg}	ρ (g/cm^3)	M_s (T) As-melt-spun	H_c (A/m) As-melt-spun	H_c (A/m) after 15 (20) min anneal	M_s (T) after 15 (20) min anneal
$Fe_{78}Mo_1B_3C_7P_{10}Si_1$	585	688	728	708	1278	0.54	7.52	1.42	18	16 (25)	1.41 (1.41)
$Fe_{78}Mo_1B_5C_5P_{10}Si_1$	589	699	739	719			7.5	1.43	15	32	1.42
$Fe_{78}Mo_1B_7C_3P_{10}Si_1$	593	703	743	723			7.47	1.44	20	400	1.37
$(Fe_{0.85}Co_{0.15})_{78}Mo_1B_3C_7P_{10}Si_1$	665	683	723	703			7.72	1.43	19	14	1.44
$(Fe_{0.8}Co_{0.2})_{78}Mo_1B_3C_7P_{10}Si_1$	683	683	723	703	1238	0.55	7.73	1.44	20	15 (20)	1.43 (1.42)
$(Fe_{0.7}Co_{0.3})_{78}Mo_1B_3C_7P_{10}Si_1$	783	680	720	700			7.76	1.38	19	22	1.37

M_s and H_c values obtained for 20 min anneal are in parenthesis.

Fig. 3. XRD scans of (a) as-spun and annealed ribbons of $Fe_{78}Mo_1B_3C_7P_{10}Si_1$ and (b) $(Fe_{0.8}Co_{0.2})_{78}Mo_1B_3C_7P_{10}Si$, obtained after each 5-min annealing interval in the SCL region. The annealing temperatures are 708 and 703 K, respectively.

$Fe_{78}Mo_1B_3C_7P_{10}Si_1$ with low boron concentration, on the other hand, still exhibits a low coercivity of 16 A/m after 15 min annealing that increases to ~25 A/m after annealing for 20 min. Fig. 3(a) shows the X-ray diffraction patterns of $Fe_{78}Mo_1B_3C_7P_{10}Si_1$ annealed for 5, 10, 15 and 20 min at 708 K. A small crystalline peak is observed after annealing for 10 min in the SCL region. The crystalline peak becomes more prominent after 15–20 min annealing. Although a comparatively low coercive field ~25 A/m is measured even after 20 min annealing, the XRD patterns indicate that the amorphous phase is thermally stable only up to about 10 min in the SCL region. A much larger crystalline peak is observed in the XRD patterns of $Fe_{78}Mo_1B_7C_3P_{10}Si_1$ after annealing for 15 min, in agreement with the higher values of H_c measured. This indicates a resistance to crystallization with an increase in carbon content, substituted for boron, in the $Fe_{78}Mo_1B_3C_7P_{10}Si_1$. This may be understood from a thermodynamic point of view, from a study by Wu et al. [17], indicating that Fe–C systems have a larger driving force for glass formation and resistance against crystallization compared to that of Fe–B systems.

Substitution of cobalt for iron in the more stable $Fe_{78}Mo_1B_3C_7P_{10}Si_1$ alloy increases M_s, resulting in a higher M_s of 1.44 T. The higher M_s value obtained near 15.6 at.% cobalt substitution indicates a shift of M_s maximum towards lower cobalt concentrations compared to the original Slater–Pauling curve [18]. However, the Curie temperature continues to increase with

cobalt substitution from $T_c \sim 585$–783 K in $Fe_{78}Mo_1B_3C_7P_{10}Si_1$ and $(Fe_{0.7}Co_{0.3})_{78}Mo_1B_3C_7P_{10}Si_1$, respectively. Meanwhile, T_x decreases with an increase in cobalt substitution. Fig. 3(b) shows the XRD patterns of $(Fe_{0.8}Co_{0.2})_{78}Mo_1B_3C_7P_{10}Si_1$ annealed up to 20 min at 703 K in the SCL region. Most of the amorphous phase is retained even after annealing for 15–20 min. Indeed, there is a remarkable suppression of crystalline peaks in the XRD patterns of the samples annealed up to 20 min. In addition, a low coercive field ~20 A/m is measured. The corresponding M_s and H_c values are shown in Table 1. The glassy ribbons of the present alloys remain flexible after 15 min annealing time, as evident by the fact that the ribbons do not break upon winding around a 1 mm diameter rod. In particular, the ribbons of $(Fe_{0.8}Co_{0.2})_{78}Mo_1B_3C_7P_{10}Si_1$ remain flexible even after 20 min annealing. Further, glassy rods of about 1 mm diameter can be obtained for $(Fe_{0.8}Co_{0.2})_{78}Mo_1B_3C_7P_{10}Si_1$ using copper mold suction casting technique. Thus, although only a moderate $\Delta T_x \sim 40$ K and $T_{rg} \sim 0.55$ are measured, high thermal stability is observed in this composition. For comparison, glassy $Fe_{75}Mo_2Ga_3P_{10}C_4B_4Si_2$ alloys reported by Shen et al. [10] showed a higher $\Delta T_x \sim 60$ K and larger $T_{rg} \sim 0.6$, and could be cast into larger rods, yet remained stable only for 10 min upon annealing at $0.37\Delta T_x$ above T_g.

Fig. 4 shows the partial time–temperature transformation (TTT) diagrams for $Fe_{78}Mo_1B_3C_7P_{10}Si_1$ and $(Fe_{0.8}Co_{0.2})_{78}Mo_1B_3C_7P_{10}Si_1$ metallic glasses focusing on the temperature range between T_g and T_x. The onset of crystallization is determined using XRD. The annealed samples are said to be fully amorphous if no crystalline peaks can be detected within the resolution of the XRD scans. Accordingly, by detecting the onset of crystallization, a solid curve is drawn to separate the amorphous region from the mixed phase region in Fig. 4. Comparing these two glassy alloys, it is noted that the solid curve for the $(Fe_{0.8}Co_{0.2})_{78}Mo_1B_3C_7P_{10}Si_1$ alloy shifts toward longer annealing times. The slopes of the TTT-curves are also different, in the two compositions as observed in Fig. 4(c), with the latter alloy showing a slightly steeper slope in the TTT plot. The slope (dT/dt) of the TTT-curves indicates the time required to reach the onset of crystallization at a given temperature interval. A gradual slope in the non-cobalt containing composition indicates less time required to reach the onset of crystallization at higher temperatures, whereas a steeper slope in the cobalt containing composition indicates more time required to reach the onset of crystallization. TEM analyses using bright field images (at a magnification of 50k×) and electron diffraction patterns of $Fe_{78}Mo_1B_3C_7P_{10}Si_1$ and $(Fe_{0.8}Co_{0.2})_{78}Mo_1B_3C_7P_{10}Si_1$, annealed at 20° above T_g for 20 min are shown in Fig. 5(a) and (b), respectively. The dramatic effect of cobalt substitution on thermal stability is evident from micrographs of the two compositions. The TEM micrograph of $(Fe_{0.8}Co_{0.2})_{78}Mo_1B_3C_7P_{10}Si_1$ indicates fewer crystallites in amorphous matrix, compared to that of $Fe_{78}Mo_1B_3C_7P_{10}Si_1$. In addition, a closer observation indicates the presence of two different types of crystallites, dendritic particles corresponding to BCC iron crystals and spherical particles corresponding to Fe-metalloid phases in $(Fe_{0.8}Co_{0.2})_{78}Mo_1B_3C_7P_{10}Si_1$. In contrast, only spherical particles are observed in $Fe_{78}Mo_1B_3C_7P_{10}Si_1$. Electron diffraction patterns of the two compositions indicate primarily amorphous phase, but a closer inspection reveals a larger number of diffraction spots in $Fe_{78}Mo_1B_3C_7P_{10}Si_1$ compared to that of $(Fe_{0.8}Co_{0.2})_{78}Mo_1B_3C_7P_{10}Si_1$. Preliminary crystallization studies using X-ray diffraction indicate a body-centered-cubic (BCC) iron phase and an iron-metalloid phase (boride, phosphide or carbide) emerging almost simultaneously in the $(Fe_{0.8}Co_{0.2})_{78}Mo_1B_3C_7P_{10}Si_1$ alloy. In contrast, in $Fe_{78}Mo_1B_3C_7P_{10}Si_1$, only iron-metalloid phases emerge.

The higher thermal stability of $(Fe_{0.8}Co_{0.2})_{78}Mo_1B_3C_7P_{10}Si_1$ in comparison with $Fe_{78}Mo_1B_3C_7P_{10}Si_1$ is not clear because of the competition between thermodynamic driving forces and kinetics that determine the formation of the BCC iron phase and iron-metalloid phases during crystallization. However, from an observational point of view, $(Fe_{0.8}Co_{0.2})_{78}Mo_1B_3C_7P_{10}Si_1$ is found to have a more densely packed atomic structure than that of $Fe_{78}Mo_1B_3C_7P_{10}Si_1$, as evident from the apparently high atomic packing density of (Fe,Co) containing alloys compared to that of Fe-containing alloys. A detailed discussion of density estimation

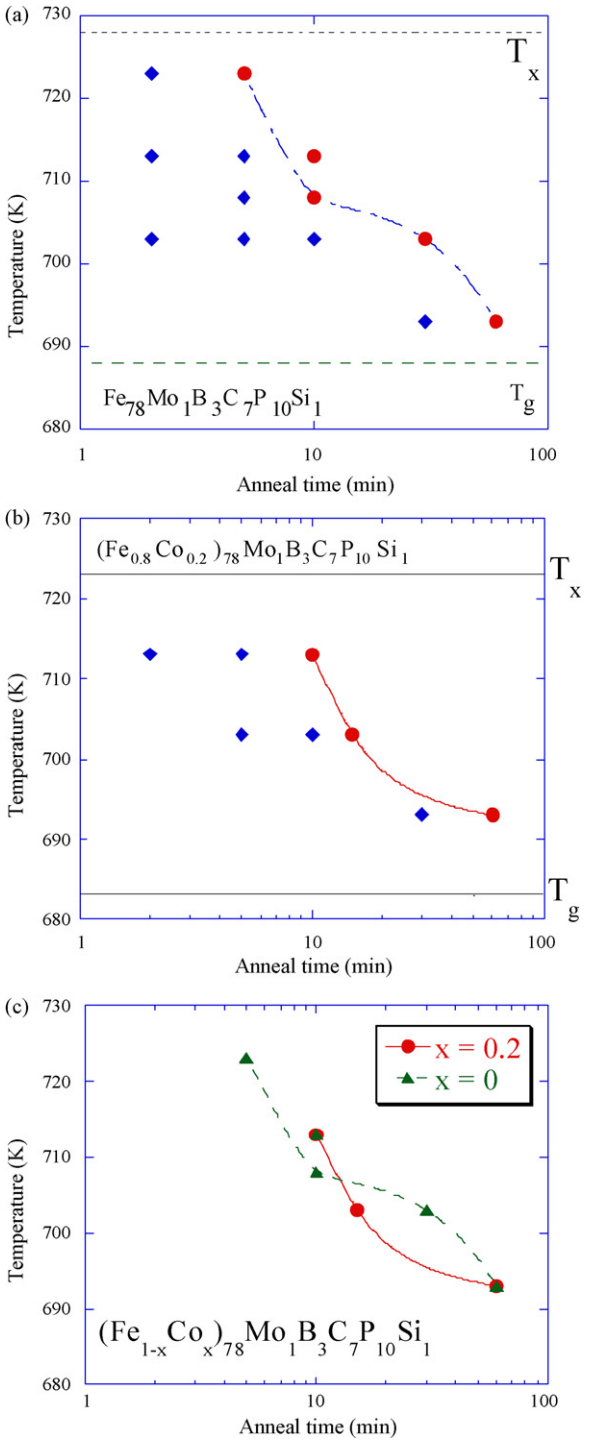

Fig. 4. Partial time–temperature transformation (TTT) diagrams of (a) $Fe_{78}Mo_1B_3C_7P_{10}Si_1$ and (b) $(Fe_{0.8}Co_{0.2})_{78}Mo_1B_3C_7P_{10}Si_1$ metallic glasses in the SCL region. The (♦) and (●) symbols in (a) and (b) are for the single amorphous phase, and mixed phase samples, respectively. The curves are guides to the eye signifying the onset of crystallization. (c) Compares the onset times of crystallization of the two compositions, plotted together.

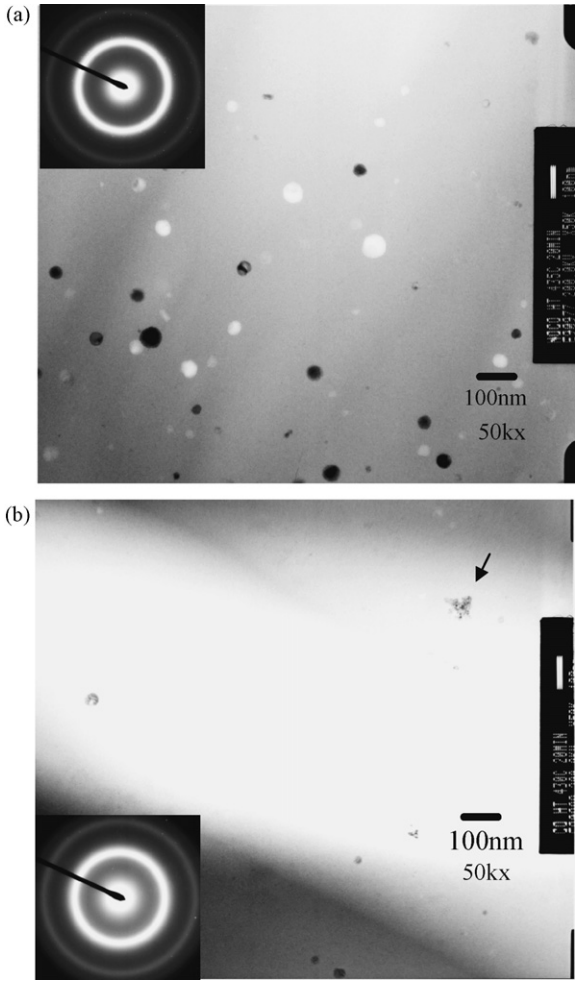

Fig. 5. TEM bright field images at a magnification of 50k× and electron diffraction patterns (insets) of (a) $Fe_{78}Mo_1B_3C_7P_{10}Si_1$ annealed at 708 K and (b) $(Fe_{0.8}Co_{0.2})_{78}Mo_1B_3C_7P_{10}Si$ annealed at 703 K, for 20 min inside the supercooled liquid region. Only spherical particles are observed in (a) while both spherical and dendritic particles are observed in (b). A dendritic crystallite is indicated by an arrow shown in (b).

in these alloys will be provided in reference [16]. As pointed out by Miracle et al. [19], a more efficiently packed atomic structure is expected to lead to a higher viscosity and consequently a reduction in the mobility of the atoms. A reduction of atomic mobility inside the SCL region is likely to slow down the process of nucleation in $(Fe_{0.8}Co_{0.2})_{78}Mo_1B_3C_7P_{10}Si_1$, compared to that of $Fe_{78}Mo_1B_3C_7P_{10}Si_1$, leading to a comparatively high thermal stability in the former. A more detailed analysis of the structure and crystallization properties will be required in order to understand the effect of cobalt on higher thermal stability in these metallic glasses.

4. Conclusions

The dependence of thermal stability in the deeply supercooled liquid region was studied as a function of boron concentration in the series of Fe–Mo–B–C–P–Si metallic glasses. The thermal stability of the alloys was found to increase significantly on replacing boron with carbon. As a result, the amorphous phase together with the low coercive field and high saturation magnetization could be retained after prolonged annealing in the deeply supercooled liquid region, despite the moderate ΔT_x and T_{rg} measured. Crystallization was further suppressed by substituting cobalt for iron. The present metallic glasses will be further developed for study of glass formation and crystallization phenomena and for potential application as soft magnetic alloys.

Acknowledgements

The authors thank Dr. Luana Iorio and Dr. Frank Johnson of GE Global Research Center for discussion and critical reading of the manuscript. This paper was prepared with the support of the U.S. Office of Naval Research under Award No. N00014-07-C-0550). However, any opinions, findings, conclusions or other recommendations expressed herein are those of the author(s) and do not necessarily reflect the views of the U.S. Office of Naval Research.

References

[1] G. Duan, A. Wiest, M. Lind, J. Li, W. Rhim, W.L. Johnson, Adv. Mater. 19 (2007) 4272.
[2] M.E. McHenry, M.A. Willard, D.E. Laughlin, Prog. Mater. Sci. 44 (1999) 291.
[3] B. Shen, M. Akiba, A. Inoue, Appl. Phys. Lett. 88 (2006) 131907.
[4] T. Zhang, F. Liu, S. Pang, R. Li, Mater. Trans. 48 (2007) 1157.
[5] R. Hasegawa, in: R. Hasegawa (Ed.), Glassy Metals: Magnetic, Chemical and Structural Properties, CRC Press, Inc., Boca Raton, FL, 1983, p. 175.
[6] L. Leuzzi, T.M. Nieuwenhuizen, Thermodynamics of the Glassy State, Taylor & Francis Group, Boca Raton, FL, 2008, p. 7.
[7] R.S. Aga, J.R. Morris, in: M. Miller, M. Liaw (Eds.), Bulk Metallic Glasses, Springer, New York, 2008, p. 65.
[8] D. Turnbull, Contemp. Phys. 10 (1969) 473.
[9] M. Xu, M.X. Quan, Z.Q. Hi, L.Z. Cheng, K.Y. He, J. Alloys Compd. 334 (2002) 238.
[10] B. Shen, M. Akiba, A. Inoue, Phys. Rev. B 73 (2006) 104204.
[11] V.I. Tkatch, S.G. Rassolov, V.V. Popov, V.Yu. Kameneva, O.A. Petrenko, Mater. Lett. 58 (2004) 2988.
[12] M. Sorescu, C.Y. Um, M.E. McHenry, L. Diamandescu, J. Non-Cryst. Solids 351 (2005) 663.
[13] X.J. Gu, S.J. Poon, G.J. Shiflet, M. Widom, Acta Mater. 56 (2008) 88.
[14] F.E. Luborsky, J.J. Becker, J.L. Walter, D.L. Martin, IEEE Trans. Mag. Mag. 16 (1980) 521.
[15] T. Bitoh, A. Makino, A. Inoue, A.L. Greer, Appl. Phys. Lett. 88 (2006) 182510.
[16] S. Bhattacharya, E.A. Lass, S.J. Poon, G.J. Shiflet, M. Rawlings, M. Daniil, M.A. Willard, in press.
[17] Y. Wu, X.D. Hui, Z.P. Lu, Z.Y. Liu, L. Liang, G.L. Chen, J. Alloys. Compd. 467 (2009) 187–190.
[18] T. Mizoguchi, K. Yamauchi, H. Miyajima, in: H.O. Hooper, A.M. de Graaf (Eds.), Amorphous Magnetism I, Plenum Press, New York, 1973, p. 325.
[19] D.B. Miracle, O.N. Senkov, W.S. Sanders, K.L. Kending, Mater. Sci. Eng. A 375–377 (2004) 150–156.